17. R. Rouse, S. Han, J. E. Lukens, *Phys. Rev. Lett.* **75**, 1614 (1995).
18. C. Cosmelli *et al.*, *Phys. Rev. Lett.* **82**, 5357 (1999).
19. S. Han, R. Rouse, J. E. Lukens, *Phys. Rev. Lett.* **76**, 3404 (1996).
20. ———, *Phys. Rev. Lett.* **84**, 1300 (2000).
21. W. Wernsdorfer, R. Sessoli, *Science* **284**, 133 (1999).
22. E. del Barco *et al.*, *Europhys. Lett.* **47**, 722 (1999).
23. M. Arndt *et al.*, *Nature* **401**, 680 (1999).
24. T. H. Oosterkamp *et al.*, *Nature* **395**, 873 (1998).
25. Y. Nakamura, C. D. Chen, J. S. Tsai, *Phys. Rev. Lett.* **79**, 2328 (1997).
26. V. Bouchiat, D. Vion, P. Joyez, D. Esteve, M. H. Devoret, *Phys. Scr.* **T76**, 165 (1998).
27. D. J. Flees, S. Han, J. E. Lukens, *J. Supercond.* **12**, 813 (1999).
28. Y. Nakamura, Yu. A. Pashkin, J. S. Tsai, *Nature* **398**, 786 (1999).
29. The small self-generated flux due to the persistent currents leads to a constant lowering of the energies. The crossing remains at $\frac{1}{2}\Phi_0$. In the discussion we take Φ_{ext} to be the total flux in the loop.
30. The sample consisted of a 5 μm by 5 μm aluminum loop with aluminum oxide tunnel junctions, microfabricated with e-beam lithography and shadow-evaporation techniques on a SiO_2 substrate. The lines of the loop were 450-nm wide and 80-nm thick. A DC-SQUID with a 7 μm by 7 μm loop was fabricated in the same layer around the inner loop. The DC-SQUID had an on-chip superconducting shunt capacitance of 2 pF and superconducting leads in a four-point configuration. The sample was mounted in a dilution refrigerator, inside a microwave-tight copper measurement box, magnetically shielded by two high-permeability metal shields and one superconducting shield. All spectroscopy measurements were taken with the temperature stabilized at 30 $\pm$ 0.05 mK. Microwaves were applied to the sample by a coaxial line, which was shorted at the end by a small loop of 5-mm diameter. This loop was positioned parallel to the sample plane at about 1 mm distance. Switching currents were measured with dedicated electronics, with repetition rates up to 9 kHz and bias currents ramped at typically 1 μA/ms. A detailed description of the fabrication and experimental techniques can be found in [C. H. van der Wal, J. E. Mooij, *J. Supercond.* **12**, 807 (1999)].
31. The inductances were estimated numerically from the geometry with a finite-element method. The value for M is in agreement with the flux signal from the inner loop (estimated from the step height in flux units in Fig. 2B) divided by I_p.
32. Deducing $\bar{I}_{SW}$ from the raw switching-current data I_{SW} concerned the following three points: (i) Because the variance in I_{SW} was much larger than the signature from the loop's flux (Fig. 2), we applied low-pass FFT-filtering in Φ_{ext} space (over 10^7 switching events for the highest trace, and $2 \cdot 10^8$ events for the lowest trace in Fig. 3A). We checked that the cutoff frequency was chosen high enough not to influence any parameters deduced from the data. (ii) By applying Φ_{ext}, we also apply flux directly to the DC-SQUID. The resulting background signal was subtracted (Fig. 2B). We checked that the estimated dip and peak positions in Fig. 3B did not depend significantly on subtracting a background signal. (iii) Applying microwaves and changing the sample temperature influenced the switching-current levels substantially. To make the flux signal of all data sets comparable, we scaled all data sets to I_{SW} = 100 nA at $\Phi_{ext} = \frac{1}{2}\Phi_0$. Any uncertainty coming from this scaling is accounted for in the error bars in Figs. 3 and 4. Data taken in the presence of microwaves could only be obtained at specific frequencies where I_{SW} was not strongly suppressed by the microwaves. At temperatures above 300 mK, drift in the I_{SW} level due to thermal instabilities of the refrigerator obscured the signal.
33. A. J. Leggett *et al.*, *Rev. Mod. Phys.* **59**, 1 (1987).
34. N. Prokof'ev, P. Stamp, *Rep. Prog. Phys.* **63**, 669 (2000) (e-Print available at http://xxx.lanl.gov/abs/cond-mat/0001080).
35. L. Tian *et al.*, in *Quantum Mesoscopic Phenomena and Mesoscopic Devices in Microelectronics, Proceedings of a NATO-ASI Workshop*, in press (e-Print available at http://xxx.lanl.gov/abs/cond-mat/9910062).
36. M. Grifoni, P. Hänggi, *Phys. Rep.* **304**, 229 (1998).
37. For an in-depth discussion on macro-realism, see the essays of A. J. Leggett and A. Shimony in *Quantum Measurement: Beyond Paradox*, R. A. Healey, G. Hellman, Eds. (Univ. of Minnesota Press, Minneapolis, 1998), pp. 1–31.
38. We thank J. B. Majer, A. C. Wallast, L. Tian, D. S. Crankshaw, J. Schmidt, A. Wallraff, L. Levitov, and D. Esteve for help and for stimulating discussions. This work was financially supported by the Dutch Foundation for Fundamental Research on Matter (FOM), the European TMR research network on superconducting nanocircuits (SUPNAN), the U.S. Army Research Office (grant DAAG55-98-1-0369), and the NEDO joint research program (NTDP-98).

11 July 2000; accepted 8 September 2000

Triple Vortex Ring Structure in Superfluid Helium II

Demosthenes Kivotides, Carlo F. Barenghi,* David C. Samuels

Superfluids such as helium II consist of two interpenetrating fluids: the normal fluid and the superfluid. The helium II vortex ring has generally been considered merely as a superfluid object, neglecting any associated motion of the normal fluid. We report a three-dimensional calculation of the coupled motion of the normal-fluid and superfluid components, which shows that the helium II vortex ring consists of a superfluid vortex ring accompanied by two coaxial normal-fluid vortex rings of opposite polarity. The three vortex rings form a coherent, dissipative structure.

Vortex rings (*1*) have long been studied as ideal examples of organized flow structures. A large body of literature has been concerned with vortex rings in a zero-viscosity (inviscid) fluid in which the vortex core thickness is much smaller than the ring's radius. This mathematical idealization is realized in a quantum fluid (*2, 3*), helium II, which is a superposition of two fluid components: the normal fluid (which is a fluid with nonzero viscosity) and the superfluid (an inviscid fluid). The concept of the superfluid vortex ring (*4*) or loop has contributed to many advances in superfluidity, ranging from vortex creation (*5, 6*) to turbulence (*7–10*). An example of this is the fundamental issue of quantum mechanical phase coherence and the onset of dissipation. Ions injected into superfluid helium II move without friction, provided that the speed does not exceed a critical value (*11*) above which superfluid vortex rings are created (*5*). Vortex creation (*12, 13*) and motion (*14, 15*) have been studied theoretically using various models and are also being investigated by atomic physicists in the context of Bose-Einstein condensation in clouds of alkaline atoms (*15, 16*). The concept of the vortex ring has been applied to interpretations of the nature of the roton (*17–19*) and the superfluid transition itself (*20*). Finally, vortex rings are important in the study of superfluid turbulence, which manifests itself as a disordered tangle of superfluid vortex loops (distorted vortex rings). Superfluid vortex lines may also end at walls, or at free surfaces, without forming closed loops. For simplicity, we will consider here a circular superfluid vortex ring, but our results should also apply to all superfluid vortex lines.

Mathematics Department, University of Newcastle, Newcastle upon Tyne NE1 7RU, UK.

*To whom correspondence should be addressed. E-mail: c.f.barenghi@ncl.ac.uk

Recent experiments, such as the observation of decay rates of superfluid vorticity (*21, 22*) consistent with the decay rates of Navier-Stokes turbulence, motivate our study of the dynamical coupling between the superfluid vorticity and the normal-fluid component. Superfluid vorticity scatters (*23*) the thermal excitations that make up the normal fluid, producing a mutual friction acting on the velocity fields $\mathbf{V}_s$ and $\mathbf{V}_n$ of the two fluid components of helium II. Although the superfluid vorticity can be detected directly by the second sound technique (*21*), very little is actually known about the normal-fluid flow because we have no practical flow visualization techniques near absolute zero. We present results of a three-dimensional calculation in which $\mathbf{V}_n$ and $\mathbf{V}_s$ are determined self-consistently. The calculation reveals the surprising triple structure of the helium II vortex ring. We also discuss the implications of this finding for the interpretation of current turbulence experiments.

Our method is based on an improvement over the vortex dynamics approach of Schwarz (*24, 25*), who modeled a superfluid vortex line as a curve $\mathbf{S}(\xi,t)$ that obeys the

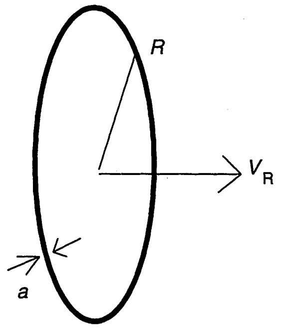

Fig. 1. Schematic representation of a superfluid vortex ring of radius R and core size $a \ll R$ lying in the x-z plane and propagating with speed V_R in the y direction. In helium II the core size a is ~0.1 nm.

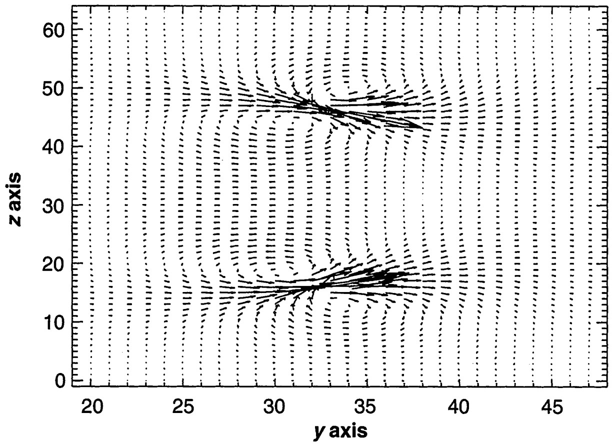

Fig. 2. Normal-fluid velocity field in the y-z plane induced by mutual friction with the superfluid vortex ring. The superfluid vortex ring cuts through the plane at the centers of the jet-like flows in the normal fluid [approximately at positions (32,17) and (32,47)]. The normal-fluid flow was calculated on a 64^3 grid. The parameter values are temperature T = 1.3 K and Reynolds number Re = $2RV_R/\nu_n$ = 1.2, where R and V_R are the initial radius and velocity of the superfluid vortex ring, respectively.

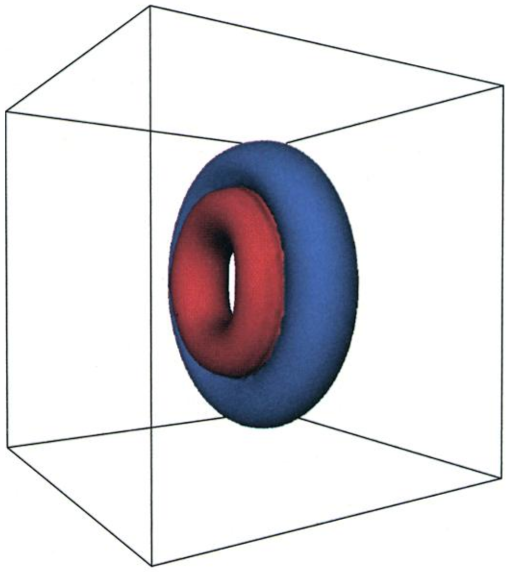

Fig. 3. Iso-surfaces of the ϕ component of the normal-fluid vorticity ω_ϕ. Positive values are blue and negative values are red, and the two iso-surfaces are set at the same magnitude of ω_ϕ. The superfluid vortex ring is oriented so that its vorticity vector defines the positive ϕ direction (the angle about the y axis). The superfluid vortex ring lies between the two normal-fluid vortices. The triple vortex structure moves to the right along the y axis and is shown from the rear. The positive (outer) normal-fluid vortex ring leads the motion, and the negative (inner) ring trails. The simulation parameters are the same as in Fig. 2.

$$\frac{d\mathbf{S}}{dt} = \mathbf{V}_s + h_2\mathbf{S}' \times (\mathbf{V}_n - \mathbf{V}_s) - h_3\mathbf{S}' \times \mathbf{S}' \times (\mathbf{V}_n - \mathbf{V}_s) \quad (1)$$

where t is time, ξ is arc length, and primes represent derivatives by arc length. For convenience, the mutual friction coefficients (*26*) h_2 and h_3 are respectively defined from the standard mutual friction coefficients D and D_t by $h_2 = \rho_s\kappa D/D_0^2 + D^2$ and $h_3 = (D^2 - D_0D_t)/(D_0^2 + D^2)$, where $D_0 = \rho_s\kappa - D_t$, κ is the quantum of circulation, and ρ_s is the density of the superfluid component. The superfluid vorticity generates a velocity $\mathbf{V}_s$ through the Biot-Savart law,

$$\mathbf{V}_s(\mathbf{x}) = \frac{\kappa}{4\pi}\int \frac{(\mathbf{S} - \mathbf{x}) \times d\mathbf{S}}{|\mathbf{S} - \mathbf{x}|^3} \quad (2)$$

where the integral extends over all superfluid vortex lines (and over image vortex lines if boundaries are present). In the absence of friction ($h_2 = h_3 = 0$) we recover the classical Euler model, in which a vortex ring of radius R moves at the self-induced speed $V_R = (\kappa/4\pi R)[\log(8R/a) - ½]$, where a is the vortex core radius. The key feature that makes our approach different from that of Schwarz is that the normal-fluid velocity $\mathbf{V}_n$ is not held fixed in this calculation, but is obtained at each time step by solving the forced Navier-Stokes equation

$$\frac{\partial \mathbf{V}_n}{\partial t} + (\mathbf{V}_n\cdot\nabla)\mathbf{V}_n = -\frac{1}{\rho}\nabla p + \nu_n\nabla^2\mathbf{V}_n + \frac{1}{\rho_n}\mathbf{F} \quad (3)$$

where ρ_n is the density of the normal-fluid component, ρ is the total density of the fluid, p is pressure, $\nu_n = \mu/\rho_n$ is the kinematic viscosity (where μ is viscosity), ∇ is the gradient operator, and $\mathbf{F}$ is the mutual friction force per unit volume. This equation is only valid when the flow is isothermal. The treatment of the motion of the excitations (the constituents of the normal fluid) as a fluid is only valid at length scales larger than the excitation mean free path (*2*).

The superfluid vortex line $\mathbf{S}$ is discretized into N mesh points (typically N = 202), and the Navier-Stokes equation is discretized into a three-dimensional grid of M^3 points in a periodic box (typically M = 64). The friction force on the normal fluid, per unit length of superfluid vortex line, is given by

$$\mathbf{f} = D\mathbf{S}' \times \mathbf{S}' \times (\mathbf{V}_n - \mathbf{V}_L) - D_t\mathbf{S}' \times (\mathbf{V}_n - \mathbf{V}_L) \quad (4)$$

where $\mathbf{V}_L = d\mathbf{S}/dt$ is the velocity of the superfluid vortex line. The mutual friction force per unit volume, $\mathbf{F} = \Sigma\mathbf{f}d\xi/\delta^3$, on each cell of the computational grid is calculated from the contributions of each segment of $\mathbf{S}$ (of length $d\xi$) that falls within that grid cell of volume δ^3. Grid cells that contain no superfluid vortex lines feel no mutual friction force.

The calculation begins with a circular superfluid vortex ring (Fig. 1) and the normal fluid at rest. As the superfluid vortex ring moves, a normal-fluid flow structure is created by the action of mutual friction. The superfluid vortex ring remains circular, and the induced normal-fluid flow structure is also axisymmetric. Our direct time-stepping of the equations of motion proves the stability of the coupled normal fluid–superfluid solution with respect to nonaxisymmetric infinitesimal disturbances. The stability of this structure was maintained even with imposed disturbances in the amplitude of the vortex ring radius of up to 10%. Further numerical experiments with an imposed uniform normal-fluid flow, U_n, in the direction of the vortex ring motion also showed that the axisymmetric shape of this coupled flow structure remains stable for both shrinking vortex rings ($U_n < V_R$) and growing rings ($U_n > V_R$).

Our most important finding concerns the nature of the normal-fluid flow structure created by the mutual friction with the superfluid vorticity. Surprisingly, this structure is not a trail or wake that slowly decays by viscous effects behind the superfluid vortex ring, but is instead a jet-like flow centered on the position of the superfluid vortex line (Fig. 2). The superfluid vortex ring is thus accompanied by two normal-fluid vortex rings: one of the same polarity and a slightly larger radius, and one of opposite polarity and a slightly smaller radius (Fig. 3). The superfluid vortex ring (not shown in the figure) is located between the outer and inner normal-fluid vortex rings, at the position of the forward jet of normal fluid visible in Fig. 2 [a similar structure has been observed by Idowu *et al.* (*27*) in a simpler two-dimensional calculation]. The normal-fluid vortex rings move along with the superfluid vortex ring, even though the largest normal-fluid velocity is always smaller than the velocity of the superfluid vortex ring, V_R. This behavior illustrates that this coupled flow structure is being continuously generated by mutual friction and dissipated rapidly by the normal-fluid viscosity. The superfluid vortex ring shrinks as it moves, providing the energy that is dissipated in the normal fluid.

We observe that the normal-fluid flow structure generated by a superfluid vortex ring moves with the superfluid vortex ring and has the same length scale. The Reynolds number defined using a length scale of $2R$ and a velocity of V_R is $\mathrm{Re} = (\kappa/\nu_n)\{[\log(8R/a) - ½]/2\pi\}$. The term in braces is close to unity for a very large range of R, and the ratio κ/ν_n is of order unity. Thus, the Reynolds number of the normal-fluid part of this flow structure is of order unity.

The qualitative form of the normal-fluid vorticity generated by the superfluid vorticity is important in the interpretation of current turbulence experiments in helium II (*21, 22, 28, 29*). It appears from our calculation that, at least in the parameter regime studied, superfluid vorticity is not able to stir the normal fluid strongly enough to make it turbulent, but rather creates a very dissipative Stokes flow in the normal fluid near the superfluid vortex lines. If we rule out this source of turbulence, then normal-fluid turbulence must then be induced by the boundaries (*21, 28, 29*) or arise from shear flow instabilities (*30*). Only in the case of shear flow instabilities could the mutual friction force with the superfluid directly affect the normal-fluid turbulence.

References and Notes

1. P. G. Saffman, *Vortex Dynamics* (Cambridge Univ. Press, Cambridge, 1992).
2. D. R. Tilley, J. Tilley, *Superfluidity and Superconductivity* (Institute of Physics, Bristol, UK, 1994).
3. R. P. Feynman, *Prog. Low Temp. Phys.* **1**, 17 (1955).
4. R. J. Donnelly, *Quantized Vortices in Helium II* (Cambridge Univ. Press, Cambridge, 1991).
5. R. M. Bowley, P. V. E. McClintock, F. E. Moss, G. G. Nancolas, P. C. E. Stamp, *Philos. Trans. R. Soc. London Ser. A* **307**, 201 (1982).
6. B. Jackson, L. F. McCann, C. S. Adams, *Phys. Rev. A* **60**, 3604 (2000).
7. S. K. Nemirovskii, W. Fiszdon, *Rev. Mod. Phys.* **67**, 37 (1995).
8. B. V. Svistunov, *Phys. Rev. B* **52**, 3647 (1995).
9. W. F. Vinen, *Phys. Rev. B* **61**, 1410 (2000).
10. D. C. Samuels, D. Kivotides, *Phys. Rev. Lett.* **83**, 5306 (1999).
11. G. W. Rayfield, F. Reif, *Phys. Rev. A* **136**, 1194 (1964).
12. C. M. Muirhead, W. F. Vinen. R. J. Donnelly, *Philos. Trans. R. Soc. London Ser. A* **311**, 433 (1984).
13. T. Frisch, Y. Pomeau, S. Rica, *Phys. Rev. Lett.* **69**, 1644 (1992).
14. P. H. Roberts, J. Grant, *J. Phys. A* **4**, 55 (1971).
15. B. Jackson, J. F. McCann, C. S. Adams, *Phys. Rev. Lett.* **80**, 3903 (1998).
16 C. Raman *et al.*, *Phys. Rev. Lett.* **83**, 2502 (1999).
17. R. J. Donnelly, in *Quantum Statistical Mechanics in the Natural Sciences*, B. Kursunoglu, S. L. Mintz, S. M. Widmayer, Eds. (Plenum, New York, 1974), pp. 359–403.
18. C. A. Jones, P. H. Roberts, *J. Phys. A* **15**, 2599 (1982).
19. L. Reatto, D. E. Galli, *Int. J. Mod. Phys.* **13**, 607 (1999).
20. G. A. Williams, *J. Low Temp. Phys.* **101**, 421 (1995).
21. M. R. Smith, R. J. Donnelly, N. Goldenfeld, W. F. Vinen, *Phys. Rev. Lett.* **71**, 2583 (1993).
22. S. R. Stalp, L. Skrebek, R. J. Donnelly, *Phys. Rev. Lett.* **82**, 4831 (1999).
23. D. C. Samuels, R. J. Donnelly, *Phys. Rev. Lett.* **65**, 187 (1990).
24. K. W. Schwarz, *Phys. Rev. B* **38**, 2398 (1988).
25. M. Tsubota, S. Maekawa, *Phys. Rev. B* **47**, 12040 (1993).
26. O. C. Idowu, D. Kivotides, C. F. Barenghi, D. C. Samuels, *J. Low Temp. Phys.* **120**, 269 (2000).
27. O. C. Idowu, A. Willis, C. F. Barenghi, D. C. Samuels, *Phys. Rev. B* **62**, 3409 (2000).
28. J. Maurer, P. Tabeling, *Europhys. Lett.* **43**, 29 (1998).
29. M. R. Smith, D. K. Hilton, S. V. VanSciver, *Phys. Fluids* **11**, 751 (1999).
30. D. J. Melotte, C. F. Barenghi, *Phys. Rev. Lett.* **80**, 4181 (1998).
31. Supported by the Leverhulme Trust. We thank W. Dobler for help with the graphics.

3 July 2000; accepted 18 September 2000

Phase Evolution in a Kondo-Correlated System

Yang Ji, M. Heiblum,* D. Sprinzak, D. Mahalu, Hadas Shtrikman

We measured the phase evolution of electrons as they traverse a quantum dot (QD) formed in a two-dimensional electron gas that serves as a localized spin. The traversal phase, determined by embedding the QD in a double path electron interferometer and measuring the quantum interference of the electron wave functions manifested by conductance oscillation as a function of a weak magnetic field, evolved by π radians, a range twice as large as theoretically predicted. As the correlation weakened, a gradual transition to the familiar phase evolution of a QD was observed. The specific phase evolution observed is highly sensitive to the onset of Kondo correlation, possibly serving as an alternative fingerprint of the Kondo effect.

The Kondo effect (*1*), a many-body phenomenon first discovered in metals slightly doped with magnetic impurities, has become one of the paradigms of strongly correlated systems. The effect, a result of an interaction between magnetic impurities with conduction electrons, leads to resonant scattering of Fermi electrons, leading to an abnormal temperature dependence of the conductivity (*2*). It was more recently recognized (*3, 4*) that the Kondo effect could also take place in a system of a spin-polarized quantum dot (QD) (*5*) strongly coupled to an electron reservoir. Goldhaber-Gordon *et al.* (*6*), and others later, observed clearly such an effect in a QD. Moreover, they were able to control in situ many relevant parameters that affect the Kondo correlation, e.g., the energy level of the localized impurity (the QD) and the coupling strength between the localized impurity and the conduction electrons. Even though the Kondo effect has been studied for some time, one of its most fundamental properties was never experimentally verified: a phase shift of $\pi/2$ experienced by electrons at the Fermi energy scattering of the many-body spin singlet (*7, 8*), known generally to take place at resonance. The phase evolution in a Kondo-correlated QD was theoretically predicted also to be $\pi/2$ at resonance (*9*). Here, we address this issue experimentally by combining a mesoscopic Kondo-correlated QD with a double path Aharonov-Bohm (AB) interferometer (*10, 11*). After verifying the coherence of the QD, we proceeded to measure the traversal phase shift of the electrons that pass through the dot.

The QD, serving as a localized spin, is a small, confined puddle of electrons, with two tunnel barriers coupling it to two electron reservoirs. The electrons in the puddle occupy a discrete ladder of energy levels, with level energy ε_d and an average energy separation Δ between non–spin-degenerate levels. A capacitively coupled metallic gate (plunger) is used to tune the energy levels in the dot. Resonant tunneling between the two reservoirs (through the tunnel barrier–dot–tunnel barrier system) occurs and current flows when an energy level in the dot is aligned with the Fermi level in the leads. When one of the electronic levels drops below the Fermi level in the leads, this level becomes occupied and the number of electrons in the dot increases by one. However, due to the small capacitance C of the QD and the discreteness of the electronic charge e, an additional clas-

Braun Center for Submicron Research, Department of Condensed Matter Physics, Weizmann Institute of Science, Rehovot 76100, Israel.

*To whom correspondence should be addressed. E-mail: Heiblum@wisemail.weizmann.ac.il